Advances in Applied Mathematics and Mechanics
Adv. Appl. Math. Mech., Vol. **9**, No. 2, pp. 407-428

DOI: 10.4208/aamm.2016.m1427
April 2017

An Immersed Finite Element Method for the Elasticity Problems with Displacement Jump

Daehyeon Kyeong and Do Young Kwak*

Korea Advanced Institute of Science and Technology, Daejeon, Korea 305-701, Korea

Received 26 January 2016; Accepted (in revised version) 29 April 2016

Abstract. In this paper, we propose a finite element method for the elasticity problems which have displacement discontinuity along the material interface using uniform grids. We modify the immersed finite element method introduced recently for the computation of interface problems having homogeneous jumps [20, 22]. Since the interface is allowed to cut through the element, we modify the standard Crouzeix-Raviart basis functions so that along the interface, the normal stress is continuous and the jump of the displacement vector is proportional to the normal stress. We construct the broken piecewise linear basis functions which are uniquely determined by these conditions. The unknowns are only associated with the edges of element, except the intersection points. Thus our scheme has fewer degrees of freedom than most of the XFEM type of methods in the existing literature [1, 8, 13]. Finally, we present numerical results which show optimal orders of convergence rates.

AMS subject classifications: 65N30, 74S05, 74B05

Key words: Elasticity problems, finite element method, Crouzeix-Raviart element, displacement discontinuity.

1 Introduction

Discontinuities often occur in many model problems in mechanics. For example, they appear along defects of devices, structures, etc. The defects (of material) may arise by pores, cracks, and inclusions. Other kinds of discontinuities can occur between two different solids which interact across a common interface. Examples of this kind are adhesive joints, frictional contacts, laminated structures, composite materials and so on. A simple example happens when two materials of distinct mechanical properties are bonded. Fast and accurate numerical methods to compute the displacements/stresses of such problems have been a challenging task.

*Corresponding author.
Email: huff@kaist.ac.kr (D. Kyeong), kdy@kaist.ac.kr (D. Y. Kwak)

There are several numerical approaches to solve linear elasticity problems by finite element methods (FEM) (see [3,7,36]). For problems with an interface, there are a few methods available. These methods may include: adaptive finite element methods (see [11, 12]), mixed finite element methods (see [30]), and discontinuous Galerkin methods (DG) (see [15, 24, 31]). All of these methods use grids aligned with the interface, which naturally induces unstructured meshes. Hence the structure of the stiffness matrix is complex, and it is difficult to design efficient solver such as multigrid method. This problem becomes more severe if one has to solve time dependent problems in which the interface may move, since it requires regeneration of the mesh for every time step.

In recent years, there have been some developments to solve interface problems using uniform grids. One approach is to use a uniform grid and conventional basis functions such as P_1/Q_1, and add some enrichment functions to them in a hope to cope the discontinuities. The so called extended finite element method (XFEM) was developed by J. Dolbow and T. Belytschko [8] to solve crack modeling problems. After its introduction, the XFEM was successively applied to solve many problems in solid mechanics, such as holes, crack and inclusions, [2,32,33]. Similar schemes were proposed by Becker et al. [1] and Hansbo et al. [13], where the authors proposed certain combined methods of XFEM and Nitsche's penalty methods for weak/strong discontinuities, respectively.

There is a different approach for solving (scalar) interface problems using uniform grids. The immersed finite element methods (IFEM) which use modified basis functions near the interface were introduced in [6, 21, 25–27] and were shown to be effective. The IFEM using Crouzeix-Raviart P_1 element were studied in [22] together with applications to mixed finite volume method. The IFEMs were used to solve various types of problems such as nonhomogeneous jumps case [5, 10, 18], parabolic equations [16], elasticity equations [17, 20, 28, 29, 34], electrical potential interface problem [4], PIC simulations in ion optics [19] and so on.

Recently, the IFEMs for elasticity problems with interface have been studied by various authors in different contexts. Lin et al. [29] solved planar elasticity problems with homogeneous interface conditions $[\mathbf{u}]_\Gamma = \mathbf{0}$ and $[\sigma(\mathbf{u})\mathbf{n}]_\Gamma = \mathbf{0}$ using IFEM based on linear/bilinear finite element. Hou et al. [17, 34] studied linear based IFEM including nonhomogeneous jumps in which they claim second order convergence in L^∞-norm. But it is well known that such elements suffer locking phenomena for the nearly incompressible case, see [9] for example. In [28], Lin et al. used Rannacher Turek element on rectangular grid for solving elasticity problems with homogeneous interface conditions. The numerical results shows optimal order convergence in H^1 and L^2 norms, but no theory was provided.

Kwak et al. [20] proposed an IFEM based on Crouziex-Raviart P_1 element with stability term to solve elasticity problems with homogeneous interface conditions, where they provided the convergence proof and the optimal numerical results in L^2 and H^1-norms. One of the differences from the above IFEMs is the addition of stability terms $\int_e \frac{\tau}{h}[\mathbf{u}][\mathbf{v}]ds$. It is well-known that the lowest order linear/bilinear element are not stable since the associated bilinear forms are not coercive [9, 14]. Brenner and Sung [3] inves-

tigated the convergence of Crouziex-Raviart P_1 element without stability term to solve elasticity equations. However, they used an orthogonal projection (to a macro element) in their bilinear form to resolve the non-coerciveness of the bilinear form. Recently, Hansbo et al. [15] showed that CR element becomes stable if the stability terms are added.

In this paper, we extend the method proposed in [20] for solving elasticity equations with spring-type non-homogeneous jumps [35] along an interface. We add four extra shape functions to the IFEM basis functions and impose non-homogeneous jump conditions for the displacement (proportional to the normal stresses). Our scheme is different from XFEM's in the sense that extra basis functions associated with the intersection points are introduced, and our element has two less degrees of freedom per element than XFEM's. Numerical experiments show that our scheme is robust in the sense that convergence rates are optimal even if the materials are nearly incompressible.

The rest of our paper is organized as follows. In the following section we introduce some notations, spaces, model problem and variational form. In Section 3, we define shape functions on interface elements satisfying the jump conditions. We provide a framework for the convergence proof based on the approximation property of the IFEM space and the consistency error estimate. In Section 4, we provide numerical examples for our IFEM scheme. Optimal convergence rate for various cases are observed. In the last section, conclusions are given.

2 Preliminaries

Let Ω be a connected, convex polygonal domain in $\mathbb{R}^2$ which is divided into two subdomains Ω^+ and Ω^- by a C^1 interface $\Gamma=\partial\Omega^+\cap\partial\Omega^-$, see Fig. 1. We assume the subdomains Ω^+ and Ω^- are occupied by two different elastic materials. For a differentiable function $\mathbf{v}=(v_1,v_2)$ and a tensor

$$\boldsymbol{\tau}=\begin{pmatrix}\tau_{11} & \tau_{12}\\ \tau_{21} & \tau_{22}\end{pmatrix},$$

we let

$$\nabla\mathbf{v}=\begin{pmatrix}\dfrac{\partial v_1}{\partial x} & \dfrac{\partial v_1}{\partial y}\\ \dfrac{\partial v_2}{\partial x} & \dfrac{\partial v_2}{\partial y}\end{pmatrix},\quad \operatorname{div}\boldsymbol{\tau}=\begin{pmatrix}\dfrac{\partial \tau_{11}}{\partial x}+\dfrac{\partial \tau_{12}}{\partial y}\\ \dfrac{\partial \tau_{21}}{\partial x}+\dfrac{\partial \tau_{22}}{\partial y}\end{pmatrix}.$$

From now on, we denote the vector variables by bold face characters and the scalar variables by normal characters. Let $p\geq 1$ and $m\geq 0$ be an integer. For any domain D, we let $W_p^m(D)$ ($H^m(D)=W_2^m(D)$) be the usual Sobolev space with (semi)-norms denoted by $|\cdot|_{m,p,D}$ and $\|\cdot\|_{m,p,D}$ ($\|\cdot\|_{m,D}=\|\cdot\|_{m,2,D}$). For any domain $D=T(\in\mathcal{T}_h)$ or $D=\Omega$, let

$$(\mathbf{N}^m(D))^2:=\{\mathbf{u}=(u_1,u_2)\in(H^m(D\cap\Omega^s))^2 \text{ for } s=+,-, \text{ and } \mathbf{u}=\mathbf{0} \text{ on } \partial\Omega\}$$

with norms

$$\|\mathbf{u}\|_{\mathbf{N}^m(D)}:=\|\mathbf{u}\|_{m,\Omega^+\cap D}+\|\mathbf{u}\|_{m,\Omega^-\cap D}.$$

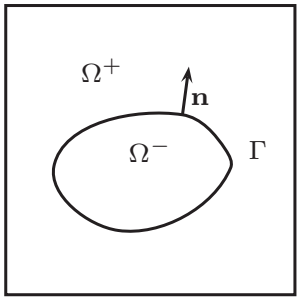

Figure 1: A domain Ω with interface.

When a finite element triangulation $\{\mathcal{T}_h\}$ is involved, the norms are understood as piecewise norms $(\sum_{T\in\mathcal{T}_h}\|\mathbf{u}\|^p_{\mathbf{N}^m(T)})^{1/p}$. If $p=2$ we denote them by $\|\mathbf{u}\|_{m,h}$ (resp. $|\mathbf{u}|_{m,h}$).

We consider the following elasticity problem having strong discontinuity along the material interface Γ: find $\mathbf{u}=(u_1,u_2)$ such that

$$-\mathrm{div}\sigma(\mathbf{u})=\mathbf{f} \quad \text{in } \Omega^s \ \ (s=+,-), \tag{2.1a}$$
$$[\mathbf{u}]_\Gamma=-R\sigma(\mathbf{u})\cdot\mathbf{n}, \tag{2.1b}$$
$$[\sigma(\mathbf{u})\mathbf{n}]_\Gamma=\mathbf{0}, \tag{2.1c}$$
$$\mathbf{u}=\mathbf{0} \quad \text{on } \partial\Omega, \tag{2.1d}$$

where

$$\sigma(\mathbf{u})=2\mu\epsilon(\mathbf{u})+\lambda tr(\epsilon(\mathbf{u}))\delta, \quad \epsilon(\mathbf{u})=\frac{1}{2}(\nabla\mathbf{u}+\nabla\mathbf{u}^T), \tag{2.2}$$

are the stress tensor and the strain tensor respectively, $\mathbf{n}$ is outward unit normal vector to Ω^+, δ is the identity tensor, and $\mathbf{f}\in(L^2(\Omega))^2$ is the external force. Here

$$\lambda=\frac{E\nu}{(1+\nu)(1-2\nu)}, \quad \mu=\frac{E}{2(1+\nu)},$$

are the Lame constants, satisfying $0<\mu_1<\mu<\mu_2$ and $0<\lambda<\infty$, and E is the Young's modulus and ν is the Poisson ratio. When the parameter $\lambda\to\infty$, this equation describes the behavior of nearly incompressible material. Since the material properties are different in each region, we set the Lamé constants $\mu=\mu^s$, $\lambda=\lambda^s$ on Ω^s for $s=+,-$. In general $\mu^+\neq\mu^-$ and $\lambda^+\neq\lambda^-$. The bracket $[\cdot]$ means the jump across the interface

$$[\mathbf{u}]_\Gamma:=\mathbf{u}|_{\Omega^+}-\mathbf{u}|_{\Omega^-}.$$

R is a second-order tensor representing the compliance of the interface. In this paper, we consider only the case of elastic isotropy, i.e., R can be written in a following form

$$R=\begin{pmatrix}\alpha+(\beta-\alpha)n_1^2 & (\beta-\alpha)n_1n_2\\ (\beta-\alpha)n_2n_1 & \alpha+(\beta-\alpha)n_2^2\end{pmatrix} \quad \text{or} \quad R_{ij}=\alpha\delta_{ij}+(\beta-\alpha)n_in_j,$$

where α and β are nonnegative constants denoting the compliance in the tangential and the normal directions of the interface, respectively (see [35]). Note that R becomes singular if either of if α or β is zero. Let the stiffness of the interface M be defined by

$$M=\begin{cases} R^{-1} & \text{for } \alpha>0, \quad \beta>0, \\ \alpha^{-1} & \text{for } \alpha>0, \quad \beta=0, \\ \beta^{-1} & \text{for } \alpha=0, \quad \beta>0, \\ 0 & \text{for } \alpha=0, \quad \beta=0, \end{cases} \tag{2.3}$$

and define the space $\mathbf{V}$ as following :

$$\mathbf{V}=\{\mathbf{v}\in\mathbf{N}^1(\Omega):[\mathbf{v}]=MR[\mathbf{v}] \text{ on } \Gamma\}. \tag{2.4}$$

Then we have the following result [13,23].

Theorem 2.1. *There exists a unique solution* $\mathbf{u}\in\mathbf{V}$ *of* (2.1a)-(2.1d) *and the solution is in* $(H^2(\Omega^s))^2$ *on each subdomain* Ω^s, $s=+,-$.

Remark 2.1. Note that the case $\alpha=\beta=0$ has been studied in [20]. If α and β are greater than zero, $\mathbf{V}$ is the same as $\mathbf{N}^1(\Omega)$.

Now we define our variational problem as follows. Find $\mathbf{u}\in\mathbf{V}$ such that

$$a(\mathbf{u},\mathbf{v})=(\mathbf{f},\mathbf{v}), \quad \forall\mathbf{v}\in\mathbf{V}, \tag{2.5}$$

where

$$a(\mathbf{u},\mathbf{v}):=\sum_{s=+,-}\Big(\int_{\Omega^s}2\mu^s\boldsymbol{\epsilon}(\mathbf{u}):\boldsymbol{\epsilon}(\mathbf{v})dx+\int_{\Omega^s}\lambda^s\mathrm{div}\mathbf{u}\mathrm{div}\mathbf{v}dx\Big)+\int_\Gamma M[\mathbf{u}][\mathbf{v}]ds.$$

As usual, $(\cdot,\cdot)$ denotes the $L^2(\Omega)$ inner product.

Theorem 2.2. *The variational problem* (2.5) *is equivalent to the original problem* (2.1a)-(2.1d).

Proof. Assume $\mathbf{u}$ satisfy (2.5) for all $\mathbf{v}\in\mathbf{V}$. Integration by parts gives

$$\sum_{s=+,-}\int_{\Omega^s}-\mathrm{div}\boldsymbol{\sigma}(\mathbf{u})\cdot\mathbf{v}dx+\int_{\partial\Omega^+}\boldsymbol{\sigma}(\mathbf{u})\mathbf{n}^+\cdot\mathbf{v}ds+\int_{\partial\Omega^-}\boldsymbol{\sigma}(\mathbf{u})\mathbf{n}^-\cdot\mathbf{v}ds+\int_\Gamma M[\mathbf{u}][\mathbf{v}]ds$$
$$=\int_\Omega\mathbf{f}\mathbf{v}dx.$$

Let $\mathbf{v}$ vanish on Γ. Then

$$\sum_{s=+,-}\int_{\Omega^s}-\mathrm{div}\boldsymbol{\sigma}(\mathbf{u})\cdot\mathbf{v}dx=\int_\Omega\mathbf{f}\mathbf{v}dx \text{ for all } \mathbf{v}\in\mathbf{V}\cap\{\mathbf{v}|_\Gamma=\mathbf{0}\}.$$

Hence it holds that

$$-\mathrm{div}\boldsymbol{\sigma}(\mathbf{u})=\mathbf{f} \quad \text{in } \Omega^+\cup\Omega^-$$

and

$$0=\int_{\partial\Omega^+}\sigma(\mathbf{u})\mathbf{n}^+\cdot\mathbf{v}ds+\int_{\partial\Omega^-}\sigma(\mathbf{u})\mathbf{n}^-\cdot\mathbf{v}ds+\int_\Gamma M[\mathbf{u}][\mathbf{v}]ds \quad \text{for all } \mathbf{v}\in\mathbf{V}.$$

Choosing $\mathbf{v}$ satisfying $\mathbf{v}^+=\mathbf{v}^-$ on Γ, we obtain

$$[\sigma(\mathbf{u})\mathbf{n}]=\mathbf{0} \quad \text{on } \Gamma.$$

Hence we obtain

$$\int_\Gamma\sigma(\mathbf{u})\mathbf{n}\cdot[\mathbf{v}]ds=-\int_\Gamma M[\mathbf{u}][\mathbf{v}]ds,$$

from which (2.1b) holds trivially when $\alpha>0$ and $\beta>0$. If $\alpha=0$ and $\beta>0$, or $\alpha>0$ and $\beta=0$, we can show the same relation using the condition $[\mathbf{v}]=MR[\mathbf{v}]$ in (2.4) and the fact that MR is idempotent.

Conversely, let $\mathbf{u}$ be the solution of the problem (2.1a)-(2.1d). Multiply (2.1a) by $\mathbf{v}\in\mathbf{V}$, integrate on each subdomain, then apply integration by parts. Using similar arguments as above, we see (2.5) holds. □

3 Numerical method

In this section, we propose a new finite element method for the elasticity problem with displacement discontinuity. It resembles an IFEM for the elasticity problem without discontinuity [20]. Let $\{\mathcal{T}_h\}$ be any (reasonable) quasi-uniform triangulations of Ω, by triangles of maximum diameter h. We do not require the mesh to be aligned with the interface. We call an element $T\in\mathcal{T}_h$ an *interface element* if the interface Γ passes through the interior of T, otherwise we call it a *noninterface* element. Let $\mathcal{T}_h^*$ be the collection of all interface elements. We assume the following situations which are easily satisfied when h is small enough:

- the interface intersects the edges of an element at no more than two points.
- the interface intersects each edge at most once, except possibly it passes through two vertices.

For simplicity, we replace the curved interface by a line segment connecting two points of intersection on each element. So on a typical triangle T (Fig. 2), we assume the interface is given by the line segment $\overline{DE}$ which divides T into two parts T^+ and T^- with $T=T^+\cup T^-\cup\overline{DE}$.

3.1 Shape functions on the interface element

The key to the immersed finite element methods for scalar elliptic problem is to paste two pieces of linear basis functions so that the newly constructed function satisfy certain interface conditions [22]. For elasticity problem with homogeneous jumps, the authors

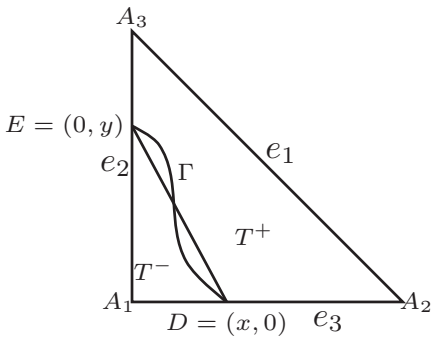

Figure 2: A typical interface triangle.

in [20] use similar idea to construct the local vector basis functions so that they satisfy the homogeneous jump conditions $[\mathbf{u}]_\Gamma=\mathbf{0}$ and $[\sigma(\mathbf{u})\mathbf{n}]_\Gamma=\mathbf{0}$.

For our problem the situation is slightly different since the jump condition (2.1b) is nonhomogeneous. Since the solution is discontinuous along the interface, we need extra degrees of freedom to take care of the discontinuity. For the basis related to the homogeneous jump, we use the same six nodal (edge based) piecewise linear functions (two copies of Crouzeix-Raviart element) as in [20]. For the nonhomogeneous jump, we need four basis functions associated with them. These are described in detail below.

For simplicity, we assume the three vertices are given by $A_1=(0,0)$, $A_2=(1,0)$ and $A_3=(0,1)$. We assume that the component of each basis function is given by two pieces of linear functions:

$$\hat{\boldsymbol{\phi}}_i(x,y)=\begin{cases}\hat{\boldsymbol{\phi}}_i^+(x,y)=\begin{pmatrix}\hat{\phi}_{i1}^+\\ \hat{\phi}_{i2}^+\end{pmatrix}=\begin{pmatrix}a_1^++b_1^+x+c_1^+y\\ a_2^++b_2^+x+c_2^+y\end{pmatrix}, & (x,y)\in T^+,\\ \hat{\boldsymbol{\phi}}_i^-(x,y)=\begin{pmatrix}\hat{\phi}_{i1}^-\\ \hat{\phi}_{i2}^-\end{pmatrix}=\begin{pmatrix}a_1^-+b_1^-x+c_1^-y\\ a_2^-+b_2^-x+c_2^-y\end{pmatrix}, & (x,y)\in T^-,\end{cases} \quad i=1,2,\cdots,10. \tag{3.1}$$

Now we assign six basis functions for the edges satisfying the homogeneous jump conditions. We need twelve conditions to determine the coefficients, six of them are the average values on the edges ; four continuity conditions (at D, E); two stress conditions along $\overline{DE}$ (Eq. (2.1c)). In other words, the basis functions $\hat{\boldsymbol{\phi}}_i=(\hat{\phi}_{i1},\hat{\phi}_{i2})$, for $i=1,2,\cdots,6$ are determined by following relations:

$$\overline{\hat{\phi}_{i1}}|e_j=\delta_{ij},\quad j=1,2,3, \tag{3.2a}$$
$$\overline{\hat{\phi}_{i2}}|e_j=\delta_{(i-3)j},\quad j=1,2,3, \tag{3.2b}$$
$$[\hat{\boldsymbol{\phi}}_i(D)]=\mathbf{0}, \tag{3.2c}$$
$$[\hat{\boldsymbol{\phi}}_i(E)]=\mathbf{0}, \tag{3.2d}$$
$$\left[\sigma(\hat{\boldsymbol{\phi}}_i)\mathbf{n}\right]_{\overline{DE}}=\mathbf{0}. \tag{3.2e}$$

Next, we consider the basis functions associated with the discontinuity of the displacement vector. In this case, the conditions are similar to the above, but the right hand sides of (3.2a), (3.2b), (3.2c) and (3.2d) are changed, respectively, to 0, 0, $(1,0)^T$ or $(0,1)^T$, etc. These twelve conditions uniquely determine the basis functions $\hat{\boldsymbol{\phi}}_i$, $i=7,\cdots,10$.

For a noninterface element T, we use $\mathbf{N}_h(T)$ to denote the space of six standard Crouzeix-Raviart basis functions associated with the edges. For an interface element T, we use $\widehat{\mathbf{N}}_h(T)$ to denote the space of functions generated by $\hat{\boldsymbol{\phi}}_i$, $i=1,\cdots,10$. Define the space $\widehat{\mathbf{V}}_h(T)$ as following :

$$\widehat{\mathbf{V}}_h(T) := \{\mathbf{v}\in\widehat{\mathbf{N}}_h(T) : [\mathbf{v}] = MR[\mathbf{v}] \text{ on } \overline{DE}\}. \tag{3.3}$$

Remark 3.1. If the constant α and β are greater than zero, then the space $\widehat{\mathbf{V}}_h(T)$ is the same as the space $\widehat{\mathbf{N}}_h(T)$. If the constant α or β is zero (but not both), then the dimension of the space $\widehat{\mathbf{V}}_h(T)$ is reduced to eight. When $\alpha=0$, then $MR=\mathbf{n}\mathbf{n}^T$, hence the conditions $[\mathbf{v}]=MR[\mathbf{v}]$ become the single condition $n_2[v_1]-n_1[v_2]=0$ at each intersection points (D and E). The case $\beta=0$ is similar.

Using these local finite element spaces, we define the global *immersed finite element space* $\widehat{\mathbf{V}}_h$ by

$$\widehat{\mathbf{V}}_h = \left\{ \begin{array}{l} \hat{\boldsymbol{\phi}}\in\widehat{\mathbf{V}}_h(T) \text{ if } T\in\mathcal{T}_h^*, \text{ and } \hat{\boldsymbol{\phi}}\in\mathbf{N}_h(T) \text{ if } T\notin\mathcal{T}_h^*; \\ \text{if } T_1 \text{ and } T_2 \text{ share an edge } e, \text{ then} \\ \int_e \hat{\boldsymbol{\phi}}|_{\partial T_1} ds = \int_e \hat{\boldsymbol{\phi}}|_{\partial T_2} ds; \text{ and } \int_{\partial T\cap\partial\Omega} \hat{\boldsymbol{\phi}} ds = \mathbf{0} \end{array} \right\}.$$

We now propose a numerical scheme for (2.1a)-(2.1d) using $\widehat{\mathbf{V}}_h$.

3.1.1 JIFEM

Find $\mathbf{u}_h\in\widehat{\mathbf{V}}_h$ such that

$$a_h(\mathbf{u}_h,\mathbf{v}_h) = (\mathbf{f},\mathbf{v}_h), \quad \forall \mathbf{v}_h\in\widehat{\mathbf{V}}_h, \tag{3.4}$$

where

$$\begin{aligned} a_h(\mathbf{u},\mathbf{v}) := & \sum_{T\in\mathcal{T}_h} \Big(\int_T 2\mu\boldsymbol{\epsilon}(\mathbf{u}):\boldsymbol{\epsilon}(\mathbf{v})dx + \int_T \lambda \mathrm{div}\mathbf{u}\mathrm{div}\mathbf{v}dx \Big) + \int_\Gamma M[\mathbf{u}][\mathbf{v}]ds \\ & + \sum_{e\in\mathcal{E}} \int_e \frac{\tau}{h}[\mathbf{u}][\mathbf{v}]ds, \quad \forall \mathbf{u},\mathbf{v}\in\widehat{\mathbf{V}}_h(\Omega). \end{aligned} \tag{3.5}$$

Here $\mathcal{E}$ denotes the collection of all the interior edges of $T\in\mathcal{T}_h$. The last terms of the above form is required in order to ensure the coercivity (see [15,20]) when nonconforming elements are used. We define the energy type norm:

$$\begin{aligned} \|\mathbf{v}\|_{a_h}^2 := & a_h(\mathbf{v},\mathbf{v}) \\ = & \sum_{T\in\mathcal{T}_h} \Big(\int_T 2\mu\boldsymbol{\epsilon}(\mathbf{v}):\boldsymbol{\epsilon}(\mathbf{v})dx + \int_T \lambda|\mathrm{div}\mathbf{v}|^2 dx \Big) + \int_\Gamma M[\mathbf{v}]^2 ds + \sum_{e\in\mathcal{E}} \int_e \frac{\tau}{h}[\mathbf{v}]^2 ds. \end{aligned} \tag{3.6}$$

It is clear that the bilinear form $a_h(\cdot,\cdot)$ is coercive by definition. Also, it is bounded, i.e.,

$$a_h(\mathbf{u},\mathbf{v}) \le C_t \|\mathbf{u}\|_{a_h} \|\mathbf{v}\|_{a_h}, \quad \forall \mathbf{u},\mathbf{v} \in \widehat{\mathbf{V}}_h + \mathbf{V}.$$

We can measure the energy type of error using the Second Strang Lemma.

Lemma 3.1 (Second Strang Lemma)**.** *There exits a constant c independent of h such that*

$$\|\mathbf{u}-\mathbf{u}_h\|_{a_h} \le c\Big(\inf_{\mathbf{v}_h \in \widehat{\mathbf{V}}_h} \|\mathbf{u}-\mathbf{v}_h\|_{a_h} + \sup_{\mathbf{w}_h \in \widehat{\mathbf{V}}_h} \frac{|a_h(\mathbf{u},\mathbf{w}_h) - a_h(\mathbf{u}_h,\mathbf{w}_h)|}{\|\mathbf{w}_h\|_{a_h}} \Big).$$

3.2 Approximation property

Now we investigate the approximation property of $\widehat{\mathbf{V}}_h$. First, let us define the interpolation operator. Assume T is an interface element. For any $\mathbf{v} = (v_1, v_2) \in \mathbf{V}(T)$, we define $I_h\mathbf{v} = (I_h v_1, I_h v_2) \in \widehat{\mathbf{V}}_h(T)$ using the average of v on each edge of T by

$$\int_{e_j} I_h v_i ds = \int_{e_j} v_i ds, \quad i=1,2, \quad j=1,2,3, \tag{3.7}$$

and the (four) jump values of $\mathbf{v}$ at the intersections of the interface and edges of T:

$$[I_h\mathbf{v}(D)] = \mathbf{v}^+(D) - \mathbf{v}^-(D), \quad [I_h\mathbf{v}(E)] = \mathbf{v}^+(E) - \mathbf{v}^-(E).$$

For noninterface element, the conditions (3.7) defines the interpolation as the usual (vector version) Crouzeix-Raviart element. We then define $I_h\mathbf{v} \in \widehat{\mathbf{V}}_h$ for $\mathbf{v} \in \mathbf{V}$ by

$$(I_h\mathbf{v})|_T = I_h(\mathbf{v}|_T) \quad \text{for each} \quad T \in \mathcal{T}_h. \tag{3.8}$$

By following the framework in Section 4.1 of [20], and noting that we have four extra degree of freedom to capture the discontinuity in this case, we can prove the following interpolation property:

Lemma 3.2. *For any $\mathbf{v} \in \mathbf{V}$, there exists a constant C_a independent of h such that*

$$\|\mathbf{v} - I_h\mathbf{v}\|_{a_h} \le C_a h \|\mathbf{v}\|_{2,h}.$$

Numerical results for interpolation are given in Section 4 to support the claim. Now we consider the consistency error. We have

Lemma 3.3. *Let $\mathbf{u} \in \mathbf{V}$ be the solution of* (2.1a)*. We assume $\sigma(\mathbf{u})\cdot\mathbf{n} \in (H^1(T))^2$ for each T. Then there exists a constant C_c independent of h such that*

$$\sup_{\mathbf{w}_h \in \widehat{\mathbf{V}}_h} \frac{|a_h(\mathbf{u},\mathbf{w}_h) - a_h(\mathbf{u}_h,\mathbf{w}_h)|}{\|\mathbf{w}_h\|_{a_h}} \le C_c h \|\mathbf{u}\|_{2,h}.$$

Proof. Sketch of the proof. We note that the consistency error term is

$$\begin{aligned}
&|a_h(\mathbf{u},\mathbf{v}_h)-a_h(\mathbf{u}_h,\mathbf{v}_h)|\\
=&|a_h(\mathbf{u},\mathbf{v}_h)-\mathbf{f}(\mathbf{v}_h)|\\
=&\Big|\sum_{T\in\mathcal{T}_h}\int_T 2\mu\epsilon(\mathbf{u}):\epsilon(\mathbf{v}_h)+\sum_{T\in\mathcal{T}_h}\int_T\lambda\mathrm{div}\mathbf{u}\mathrm{div}\mathbf{v}_h+\sum_{e\in\mathcal{E}}\int_e\frac{2\mu}{h}[\mathbf{u}][\mathbf{v}_h]ds\\
&+\int_\Gamma M[\mathbf{u}][\mathbf{v}_h]ds+\sum_{T\in\mathcal{T}_h}(\mathrm{div}\sigma(\mathbf{u}),\mathbf{v}_h)_T\Big|\\
=&\Big|\sum_{T\in\mathcal{T}_h}\Big(-(\mathrm{div}\sigma(\mathbf{u}),\mathbf{v}_h)_T+\int_{\partial T}\sigma(\mathbf{u})\mathbf{n}\cdot\mathbf{v}_h\Big)+\sum_{s=+,-}\int_\Gamma\sigma(\mathbf{u}^s)\mathbf{n}^s\cdot\mathbf{v}_h^s ds\\
&+\sum_{e\in\mathcal{E}}\int_e\frac{2\mu}{h}[\mathbf{u}][\mathbf{v}_h]ds+\int_\Gamma M[\mathbf{u}][\mathbf{v}_h]ds+\sum_{T\in\mathcal{T}_h}(\mathrm{div}\sigma(\mathbf{u}),\mathbf{v}_h)_T\Big|\\
=&\Big|\sum_{T\in\mathcal{T}_h}\int_{\partial T}\sigma(\mathbf{u})\mathbf{n}\cdot\mathbf{v}_h\Big|=\Big|\sum_{e\in\mathcal{E}}\int_e\sigma(\mathbf{u})\mathbf{n}\cdot[\mathbf{v}_h]ds\Big|,
\end{aligned}$$

where we used integration by parts and the fact that $[\mathbf{u}]=0$ across each edge and

$$\sum_{s=+,-}\int_\Gamma\sigma(\mathbf{u}^s)\mathbf{n}^s\cdot\mathbf{v}_h^s ds+\int_\Gamma M[\mathbf{u}][\mathbf{v}_h]ds=0.$$

The rest of the proof follows by the same argument in Section 4.2 of [20]. □

Now we are ready to proof the $\|\cdot\|_{a_h}$ error estimate.

Theorem 3.1. *Let* $\mathbf{u}$ *(resp.* $\mathbf{u}_h$*) be the solution of* (2.1a) *(resp.* (3.4)*). Assume that Lemma 3.3 and Lemma 3.2 hold. Then we have*

$$\|\mathbf{u}-\mathbf{u}_h\|_{a_h}\le Ch\|\mathbf{u}\|_{2,h}$$

for some constant $C>0$.

Proof. By the coercivity of the bilinear form and Lemma 3.3, we have

$$\begin{aligned}
\|\mathbf{u}_h-I_h\mathbf{u}\|_{a_h}^2=&a_h(\mathbf{u}_h-I_h\mathbf{u},\mathbf{u}_h-I_h\mathbf{u})\\
=&a_h(\mathbf{u}-I_h\mathbf{u},\mathbf{u}_h-I_h\mathbf{u})+a_h(\mathbf{u}_h-\mathbf{u},\mathbf{u}_h-I_h\mathbf{u})\\
\le&C_t\|\mathbf{u}-I_h\mathbf{u}\|_{a_h}\|\mathbf{u}_h-I_h\mathbf{u}\|_{a_h}+C_ch\|\mathbf{u}\|_{2,h}\|\mathbf{u}_h-I_h\mathbf{u}\|_{a_h},
\end{aligned}$$

and it follows that

$$\|\mathbf{u}_h-I_h\mathbf{u}\|_{a_h}\le C_t\|\mathbf{u}-I_h\mathbf{u}\|_{a_h}+C_ch\|\mathbf{u}\|_{2,h}.$$

Finally, by Lemma 3.2 and triangular inequality, we have

$$\begin{aligned}
\|\mathbf{u}-\mathbf{u}_h\|_{a_h}\le&\|\mathbf{u}_h-I_h\mathbf{u}\|_{a_h}+\|\mathbf{u}-I_h\mathbf{u}\|_{a_h}\\
\le&(C_t+1)\|\mathbf{u}-I_h\mathbf{u}\|_{a_h}+C_ch\|\mathbf{u}\|_{2,h}\\
\le&Ch\|\mathbf{u}\|_{2,h}.
\end{aligned}$$

Thus, we complete the proof. □

4 Numerical results

In this section, we provide some numerical examples. In all of the experiments, the domain $(-1,1)\times(-1,1)$ is partitioned by uniform rectangles with sizes $h_x = h_y = 1/2^{n-1}$, for $n = 1,2,\cdots$, which are again cut along diagonals. In order to describe the interface, we use the level-set function $\phi(x)$. In all of the graphs in these examples, we draw the first component of the solution $\mathbf{u}_h$ on the left column, while the right column shows the vector plot of $\mathbf{u}_h$. We also report the interpolation error using separate tables for each example.

Example 4.1. In this example, we test three sets of parameters with line interface. The level-set function, and the solution u are given as follows:

$$\begin{aligned}
&\phi(x,y) = x - y - c,\\
&\mathbf{u}^-(x,y) = \Big(\frac{x^2-y^2}{\mu^-}, \frac{x^2-y^2}{\mu^-}\Big),\\
&\mathbf{u}^+(x,y) = \Big(\frac{x^2-y^2}{\mu^+} + \sqrt{2}c\beta\frac{\lambda^+}{\mu^+}, \frac{x^2-y^2}{\mu^+} - \sqrt{2}c\beta\frac{\lambda^+}{\mu^+}\Big).
\end{aligned}$$

(a) We choose $\alpha = 0.7$, $\beta = 0.3$, $\mu^- = 100$, $\mu^+ = 1$, $\nu = 0.49$ and $c = 0.999949$.

(b) We choose $\alpha = 0.04$, $\beta = 0.08$, $\mu^- = 10$, $\mu^+ = 1$, $\nu = 0.4$ and $c = 0.062854$.

(c) We choose $\alpha = 0.6$, $\beta = 0.4$, $\mu^- = 1000$, $\mu^+ = 1$, $\nu = 0.25$ and $c = 0.849378$.

(d) We choose $\alpha = 0.4$, $\beta = 0.6$, $\mu^- = 1000$, $\mu^+ = 1$, $\nu = 0.499$ and $c = 0.566252$.

(e) We choose $\alpha = 0.64$, $\beta = 0.39$, $\mu^- = 100$, $\mu^+ = 1$, $\nu = 0.4999$ and $c = 0.9194239$.

Table 1 shows the convergence behavior of our numerical schemes. And Table 2 which is the case of nearly incompressible shows the convergence behavior also. In all the cases, we see optimal orders of convergence in L^2, H^1 and divergence norms. So our scheme is working property even if Poisson ratio approaches $1/2$. First components of the solution and vector plot of $\mathbf{u}$ are present in Fig. 3. We have listed the interpolation error in the Table 3.

Example 4.2. In this example, we test three sets of parameters with circle interface. The level-set function, and the solution $\mathbf{u}$ are given as follows:

$$\begin{aligned}
&\phi(x,y) = x^2 + y^2 - r_0^2,\\
&\mathbf{u}^-(x,y) = \Big(\frac{x^2-y^2}{\mu^-}, \frac{x^2-y^2}{\mu^-}\Big),\\
&\mathbf{u}^+(x,y) = \Big(\frac{x^2-y^2}{\mu^+} + \Big(\frac{1}{\mu^+} - \frac{1}{\mu^-}\Big)\frac{r_0^2}{2}, \frac{x^2-y^2}{\mu^+} - \Big(\frac{1}{\mu^+} - \frac{1}{\mu^-}\Big)\frac{r_0^2}{2}\Big).
\end{aligned}$$

Table 1: Example 4.1.

	$N_x \times N_y$	$\|\mathbf{u}-\mathbf{u}_h\|_{0,h}$	order	$\|\mathrm{div}\mathbf{u}-\mathrm{div}\mathbf{u}_h\|_{0,h}$	order	$\|\mathbf{u}-\mathbf{u}_h\|_{1,h}$	order
Example 4.1(a)	16 × 16	2.697e-2	-	6.950e-2	-	5.370e-1	-
	32 × 32	6.311e-3	2.095	3.542e-2	0.973	2.384e-1	1.172
	64 × 64	1.523e-3	2.051	1.788e-2	0.986	1.125e-1	1.084
	128 × 128	3.739e-4	2.026	8.981e-3	0.993	5.469e-2	1.040
	256 × 256	9.261e-5	2.013	4.501e-3	0.997	2.699e-2	1.019
	512 × 512	2.304e-5	2.007	2.253e-3	0.998	1.341e-2	1.009
Example 4.1(b)	16 × 16	2.380e-3	-	1.382e-1	-	1.675e-1	-
	32 × 32	6.116e-4	1.957	6.961e-2	0.990	8.402e-2	0.995
	64 × 64	1.484e-4	2.043	3.498e-2	0.993	4.201e-2	1.000
	128 × 128	3.644e-5	2.026	1.753e-2	0.996	2.100e-2	1.001
	256 × 256	9.022e-6	2.014	8.777e-3	0.998	1.050e-2	1.000
	512 × 512	2.244e-6	2.007	4.391e-3	0.999	5.247e-3	1.000
Example 4.1(c)	16 × 16	1.823e-3	-	8.051e-2	-	9.978e-2	-
	32 × 32	4.604e-4	1.985	4.082e-2	0.980	5.001e-2	0.996
	64 × 64	1.157e-4	1.992	2.060e-2	0.987	2.512e-2	0.994
	128 × 128	2.907e-5	1.994	1.034e-2	0.995	1.260e-2	0.995
	256 × 256	7.280e-6	1.997	5.179e-3	0.997	6.315e-3	0.997
	512 × 512	1.822e-6	1.999	2.592e-3	0.998	3.159e-3	0.999

Table 2: Example 4.1 when the materials are nearly incompressible ($\nu=0.499$, $\nu=0.4999$).

	$N_x \times N_y$	$\|\mathbf{u}-\mathbf{u}_h\|_{0,h}$	order	$\|\mathrm{div}\mathbf{u}-\mathrm{div}\mathbf{u}_h\|_{0,h}$	order	$\|\mathbf{u}-\mathbf{u}_h\|_{1,h}$	order
Example 4.1(d)	16 × 16	9.585e-2	-	1.003e-1	-	1.902e-0	-
	32 × 32	2.254e-2	2.089	5.109e-2	0.973	8.579e-1	1.149
	64 × 64	5.577e-3	2.015	2.571e-2	0.991	4.158e-1	1.045
	128 × 128	1.389e-3	2.006	1.289e-2	0.996	2.046e-1	1.023
	256 × 256	3.466e-4	2.002	6.455e-3	0.998	1.015e-1	1.012
	512 × 512	8.666e-5	2.000	3.231e-3	0.999	5.045e-2	1.007
Example 4.1(e)	16 × 16	4.437e-1	-	7.545e-2	-	8.430e-0	-
	32 × 32	1.027e-1	2.112	3.837e-2	0.975	3.634e-0	1.214
	64 × 64	2.397e-2	2.099	1.942e-2	0.982	1.710e-0	1.088
	128 × 128	5.851e-3	2.035	9.748e-3	0.995	8.313e-1	1.040
	256 × 256	1.439e-3	2.024	4.888e-3	0.996	4.072e-1	1.029
	512 × 512	3.579e-4	2.007	2.447e-3	0.998	2.033e-1	1.002

(a) We choose $\alpha=\beta=0.0891$, $\mu^-=100$, $\mu^+=1$, $\nu=0.25$ and $r_0=0.36$.

(b) We choose $\alpha=\beta=0.1035$, $\mu^-=10$, $\mu^+=1$, $\nu=0.25$ and $r_0=0.46$.

(c) We choose $\alpha=\beta=0.14985$, $\mu^-=1000$, $\mu^+=1$, $\nu=0.25$ and $r_0=0.6$.

Table 4 shows the convergence behavior. In all the cases, we see optimal orders of convergence in L^2, H^1 and divergence norms also. Plots are shown in Fig. 4. The interpolation error is shown in the Table 5.

Table 3: Interpolation error of Example 4.1.

	$N_x \times N_y$	$\|\mathbf{u}-I_h\mathbf{u}\|_{0,h}$	order	$\|\mathrm{div}\mathbf{u}-\mathrm{div}I_h\mathbf{u}\|_{0,h}$	order	$\|\mathbf{u}-I_h\mathbf{u}\|_{1,h}$	order
Example 4.1(a)	16×16	9.227e-4	-	6.913e-2	-	8.322e-2	-
	32×32	2.219e-4	2.056	3.534e-2	0.968	4.165e-2	0.999
	64×64	5.434e-5	2.030	1.786e-2	0.985	2.083e-2	0.999
	128×128	1.344e-5	2.015	8.978e-3	0.992	1.042e-2	1.000
	256×256	3.342e-6	2.008	4.501e-3	0.996	5.210e-3	1.000
	512×512	8.333e-7	2.004	2.253e-3	0.998	2.605e-3	1.000
Example 4.1(b)	16×16	1.751e-3	-	1.381e-1	-	1.620e-1	-
	32×32	4.341e-4	2.012	6.968e-2	0.987	8.098e-2	1.000
	64×64	1.060e-4	2.033	3.500e-2	0.994	4.054e-2	0.998
	128×128	2.619e-5	2.018	1.754e-2	0.997	2.028e-2	0.999
	256×256	6.507e-6	2.009	8.778e-3	0.998	1.014e-2	1.000
	512×512	1.622e-6	2.004	4.391e-3	0.999	5.072e-3	1.000
Example 4.1(c)	16×16	1.031e-3	-	8.051e-2	-	9.504e-2	-
	32×32	2.540e-4	2.022	4.090e-2	0.977	4.772e-2	0.994
	64×64	6.245e-5	2.024	2.062e-2	0.988	2.389e-2	0.998
	128×128	1.544e-5	2.016	1.034e-2	0.995	1.197e-2	0.997
	256×256	3.839e-6	2.007	5.180e-3	0.998	5.990e-3	0.999
	512×512	9.581e-7	2.003	2.593e-3	0.999	2.995e-3	1.000
Example 4.1(d)	16×16	1.966e-3	-	1.000e-1	-	1.202e-1	-
	32×32	4.843e-4	2.021	5.101e-2	0.971	5.968e-2	1.010
	64×64	1.206e-4	2.005	2.569e-2	0.990	2.985e-2	0.999
	128×128	3.013e-5	2.002	1.289e-2	0.995	1.493e-2	0.999
	256×256	7.539e-6	1.999	6.454e-3	0.998	7.470e-3	0.999
	512×512	1.884e-6	2.001	3.230e-3	0.998	3.734e-3	1.000
Example 4.1(e)	16×16	1.461e-3	-	7.525e-2	-	9.046e-2	-
	32×32	3.717e-4	1.975	3.832e-2	0.974	4.545e-2	0.993
	64×64	9.127e-5	2.026	1.941e-2	0.981	2.262e-2	1.007
	128×128	2.289e-5	1.995	9.744e-3	0.994	1.132e-2	0.998
	256×256	5.711e-6	2.003	4.887e-3	0.995	5.656e-3	1.001
	512×512	1.427e-6	2.001	2.447e-3	0.998	2.828e-3	1.000

Example 4.3. In this example, we test four sets of parameters with $\beta=0$. The level-set function ϕ and the solution $\mathbf{u}$ are given as follows:

$$\phi(x,y)=\frac{x}{2}-y-c,$$
$$\mathbf{u}^-(x,y)=\Big(\frac{(\frac{x}{2}-y)^2}{\mu^-},\frac{(\frac{x}{2}-y)^2}{\mu^-}\Big),$$
$$\mathbf{u}^+(x,y)=\Big(\frac{(\frac{x}{2}-y)^2}{\mu^+}-\Big(\frac{1}{\mu^+}-\frac{1}{\mu^-}\Big)c^2+\alpha c\frac{6}{5}\sqrt{5},\frac{(\frac{x}{2}-y)^2}{\mu^+}-\Big(\frac{1}{\mu^+}-\frac{1}{\mu^-}\Big)c^2+\alpha c\frac{3}{5}\sqrt{5}\Big).$$

(a) We choose $\alpha=0.06$, $\beta=0$, $\mu^-=100$, $\mu^+=1$, $c=0.36$ and $\nu=0.49$.

(b) We choose $\alpha=0.04$, $\beta=0$, $\mu^-=10$, $\mu^+=1$, $c=0.26$ and $\nu=0.3$.

(c) We choose $\alpha=0.6$, $\beta=0$, $\mu^-=100$, $\mu^+=1$, $c=0.79$ and $\nu=0.25$.

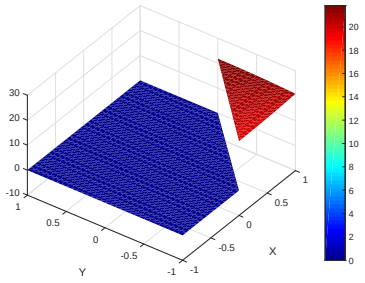

x-component of u for Example 4.1(a)

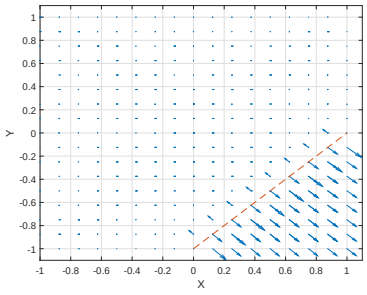

vector plot of u for Example 4.1(a)

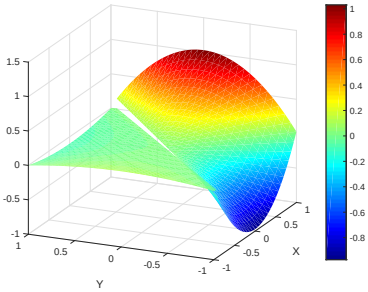

x-component of u for Example 4.1(b)

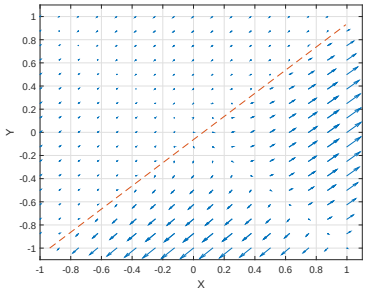

vector plot of u for Example 4.1(b)

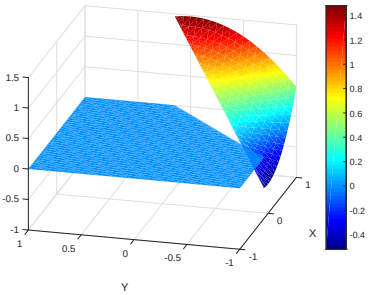

x-component of u for Example 4.1(c)

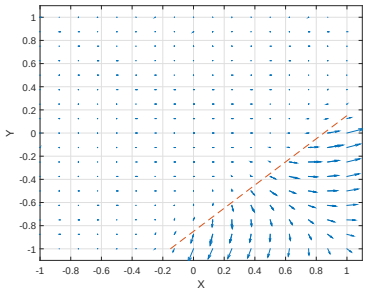

vector plot of u for Example 4.1(c)

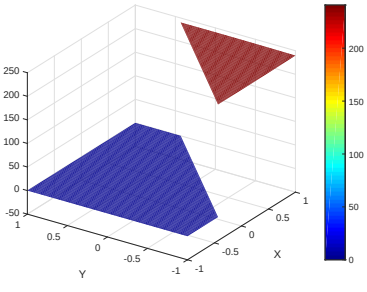

x-component of u for Example 4.1(d)

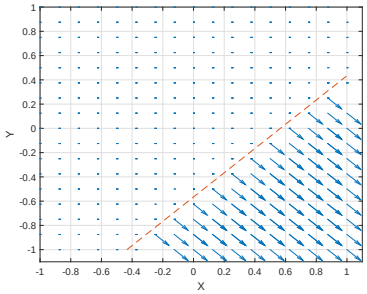

vector plot of u for Example 4.1(d)

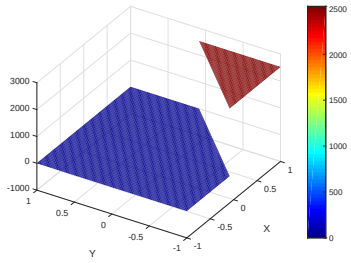

x-component of u for Example 4.1(e)

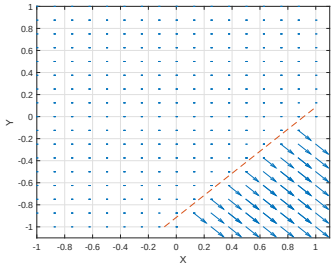

vector plot of u for Example 4.1(e)

Figure 3: Line interface, plots of u for Example 4.1.

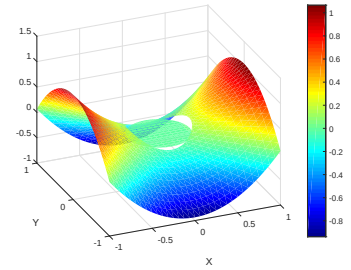

x-component of **u** for Example 4.2(a)

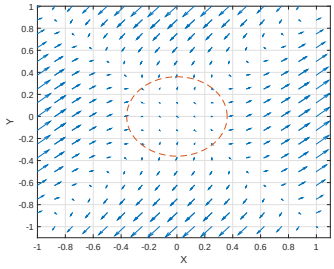

vector plot of **u** for Example 4.2(a)

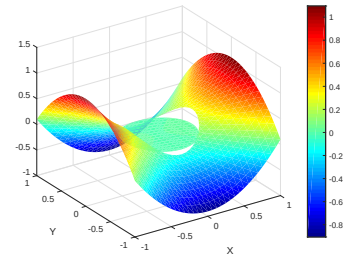

x-component of **u** for Example 4.2(b)

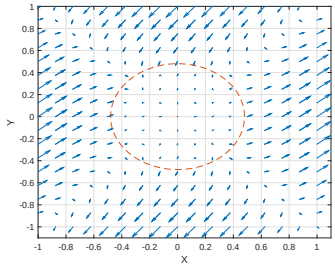

vector plot of **u** for Example 4.2(b)

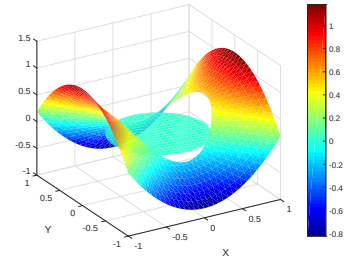

x-component of **u** for Example 4.2(c)

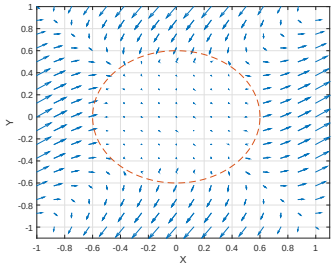

vector plot of **u** for Example 4.2(c)

Figure 4: Circle interface, plots of u for Example 4.2.

Table 4: Example 4.2.

	$N_x \times N_y$	$\|\mathbf{u}-\mathbf{u}_h\|_{0,h}$	order	$\|\mathrm{div}\mathbf{u}-\mathrm{div}\mathbf{u}_h\|_{0,h}$	order	$\|\mathbf{u}-\mathbf{u}_h\|_{1,h}$	order
Example 4.2(a)	16×16	4.928e-3	-	1.930e-1	-	2.357e-1	-
	32×32	1.244e-3	1.986	9.660e-2	0.999	1.177e-1	1.003
	64×64	3.066e-4	2.021	4.831e-2	0.999	5.885e-2	1.000
	128×128	7.866e-5	1.963	2.417e-2	0.999	2.945e-2	0.999
	256×256	2.017e-5	1.964	1.209e-2	1.000	1.473e-2	1.000
	512×512	4.970e-6	2.021	6.045e-3	1.000	7.365e-3	1.000
Example 4.2(b)	16×16	4.977e-3	-	1.856e-1	-	2.267e-1	-
	32×32	1.213e-3	2.037	9.304e-2	0.997	1.133e-1	1.001
	64×64	3.087e-4	1.974	4.659e-2	0.998	5.676e-2	0.998
	128×128	7.756e-5	1.993	2.331e-2	0.999	2.839e-2	0.999
	256×256	1.951e-5	1.991	1.166e-2	0.999	1.420e-2	0.999
	512×512	4.822e-6	2.017	5.830e-3	1.000	7.103e-3	1.000
Example 4.2(c)	16×16	4.937e-3	-	1.715e-1	-	2.095e-1	-
	32×32	1.205e-3	2.034	8.597e-2	0.997	1.048e-1	1.000
	64×64	3.328e-4	1.857	4.313e-2	0.995	5.256e-2	0.995
	128×128	7.945e-5	2.067	2.158e-2	0.999	2.629e-2	0.999
	256×256	1.960e-5	2.019	1.080e-2	0.999	1.316e-2	0.999
	512×512	4.979e-6	1.977	5.401e-3	1.000	6.580e-3	1.000

Table 5: Interpolation error of Example 4.2.

	$N_x \times N_y$	$\|\mathbf{u}-I_h\mathbf{u}\|_{0,h}$	order	$\|\mathrm{div}\mathbf{u}-\mathrm{div}I_h\mathbf{u}\|_{0,h}$	order	$\|\mathbf{u}-I_h\mathbf{u}\|_{1,h}$	order
Example 4.2(a)	16×16	2.317e-3	-	1.929e-1	-	2.233e-1	-
	32×32	5.741e-4	2.064	9.650e-2	0.999	1.116e-1	1.001
	64×64	1.431e-4	2.013	4.830e-2	0.999	5.581e-2	1.000
	128×128	3.571e-5	2.003	2.417e-2	0.999	2.792e-2	0.999
	256×256	8.915e-5	2.002	1.209e-2	1.000	1.396e-2	1.000
	512×512	2.223e-6	2.001	6.045e-3	1.000	6.981e-3	1.000
Example 4.2(b)	16×16	2.258e-3	-	1.853e-1	-	2.146e-1	-
	32×32	5.569e-3	2.016	9.299e-2	0.995	1.075e-1	0.997
	64×64	1.380e-4	2.013	4.658e-2	0.997	5.382e-2	0.998
	128×128	3.446e-5	2.002	2.331e-2	0.999	2.692e-2	0.999
	256×256	8.600e-6	2.002	1.166e-2	0.999	1.346e-2	1.000
	512×512	2.149e-6	2.001	5.830e-3	1.000	6.732e-3	1.000
Example 4.2(c)	16×16	2.099e-3	-	1.713e-1	-	1.990e-1	-
	32×32	5.194e-3	2.014	8.594e-2	0.995	9.953e-2	0.999
	64×64	1.284e-4	2.016	4.315e-2	0.994	4.989e-2	0.996
	128×128	3.198e-5	2.006	2.158e-2	0.999	2.494e-2	1.000
	256×256	7.975e-6	2.003	1.080e-2	0.999	1.247e-2	1.000
	512×512	1.992e-6	2.001	5.401e-3	1.000	6.237e-3	1.000

(d) We choose $\alpha = 0.03$, $\beta = 0$, $\mu^- = 1000$, $\mu^+ = 1$, $c = 0.52$ and $\nu = 0.4$.

(e) We choose $\alpha = 0.04$, $\beta = 0$, $\mu^- = 1000$, $\mu^+ = 1$, $c = 0.67$ and $\nu = 0.499$.

(f) We choose $\alpha = 0.36$, $\beta = 0$, $\mu^- = 100$, $\mu^+ = 1$, $c = 0.74$ and $\nu = 0.4999$.

Table 6 shows the convergence behavior of our numerical schemes. And Table 7 which is

Table 6: Example 4.3.

	$N_x \times N_y$	$\|\mathbf{u}-\mathbf{u}_h\|_{0,h}$	order	$\|\mathrm{div}\mathbf{u}-\mathrm{div}\mathbf{u}_h\|_{0,h}$	order	$\|\mathbf{u}-\mathbf{u}_h\|_{1,h}$	order
Example 4.3(a)	16×16	2.434e-2	-	4.347e-2	-	4.714e-1	-
	32×32	6.212e-3	1.970	2.188e-2	0.990	2.337e-1	1.013
	64×64	1.567e-3	1.987	1.100e-2	0.992	1.165e-1	1.004
	128×128	3.950e-4	1.988	5.514e-3	0.996	5.850e-2	0.994
	256×256	9.917e-5	1.994	2.761e-3	0.998	2.933e-2	0.996
	512×512	2.484e-5	1.997	1.381e-3	0.999	1.468e-2	0.998
Example 4.3(b)	16×16	3.074e-3	-	5.263e-2	-	1.604e-1	-
	32×32	7.872e-4	1.965	2.658e-2	0.985	8.117e-2	0.982
	64×64	1.976e-4	1.994	1.334e-2	0.995	4.082e-2	0.992
	128×128	5.018e-5	1.977	6.701e-3	0.993	2.047e-2	0.995
	256×256	1.254e-5	2.000	3.354e-3	0.998	1.025e-2	0.998
	512×512	3.146e-6	1.995	1.679e-3	0.999	5.130e-3	0.999
Example 4.3(c)	16×16	1.426e-3	-	3.104e-2	-	9.058e-2	-
	32×32	3.845e-4	1.891	1.615e-2	0.942	4.684e-2	0.951
	64×64	8.841e-5	2.121	7.949e-3	1.023	2.353e-2	0.993
	128×128	2.270e-5	1.962	4.019e-3	0.984	1.186e-2	0.988
	256×256	5.537e-6	2.035	2.005e-3	1.003	5.938e-3	0.998
	512×512	1.369e-6	2.016	1.001e-3	1.002	2.971e-3	0.999
Example 4.3(d)	16×16	3.068e-3	-	4.152e-2	-	1.315e-1	-
	32×32	7.163e-4	2.099	2.000e-2	1.054	6.589e-2	0.997
	64×64	1.900e-4	1.914	1.011e-2	0.985	3.330e-2	0.985
	128×128	4.612e-5	2.043	5.020e-3	1.009	1.664e-2	1.001
	256×256	1.176e-5	1.971	2.519e-3	0.995	8.344e-3	0.996
	512×512	2.911e-6	2.014	1.258e-3	1.002	4.171e-3	1.000

Table 7: Example 4.3 when the materials are nearly incompressible ($\nu = 0.499$, $\nu = 0.4999$).

	$N_x \times N_y$	$\|\mathbf{u}-\mathbf{u}_h\|_{0,h}$	order	$\|\mathrm{div}\mathbf{u}-\mathrm{div}\mathbf{u}_h\|_{0,h}$	order	$\|\mathbf{u}-\mathbf{u}_h\|_{1,h}$	order
Example 4.3(e)	16×16	2.766e-2	-	3.185e-2	-	6.131e-1	-
	32×32	6.905e-3	2.002	1.608e-2	0.986	2.810e-1	1.013
	64×64	1.834e-3	1.913	8.114e-3	0.987	1.367e-1	1.040
	128×128	4.749e-4	1.949	4.068e-3	0.996	6.677e-2	1.034
	256×256	1.218e-4	1.964	2.037e-3	0.998	3.289e-2	1.021
	512×512	3.091e-5	1.978	1.020e-3	0.998	1.632e-2	1.011
Example 4.3(f)	16×16	1.472e-1	-	2.862e-2	-	3.156e-0	-
	32×32	3.533e-2	2.059	1.461e-2	0.970	1.381e-0	1.192
	64×64	8.695e-3	2.022	7.357e-3	0.990	6.454e-1	1.098
	128×128	2.150e-3	2.016	3.700e-3	0.992	3.168e-1	1.026
	256×256	5.319e-4	2.015	1.853e-3	0.997	1.554e-1	1.028
	512×512	1.322e-4	2.009	9.279e-4	0.998	7.730e-2	1.007

the case of nearly incompressible shows the convergence behavior also. In all the cases, we see optimal orders of convergence in L^2, H^1 and divergence norms. So there is no locking phenomena. Optimal order of the interpolation operator when $\beta = 0$ case is also shown in the Table 8.

Table 8: Interpolation error of Example 4.3.

	$N_x \times N_y$	$\|\mathbf{u}-I_h\mathbf{u}\|_{0,h}$	order	$\|\mathrm{div}\mathbf{u}-\mathrm{div}I_h\mathbf{u}\|_{0,h}$	order	$\|\mathbf{u}-I_h\mathbf{u}\|_{1,h}$	order
Example 4.3(a)	16×16	2.333e-3	-	4.289e-2	-	1.356e-1	-
	32×32	5.929e-4	1.977	2.175e-2	0.980	6.878e-2	0.980
	64×64	1.499e-4	1.984	1.095e-2	0.990	3.464e-2	0.990
	128×128	3.732e-5	2.006	5.495e-3	0.995	1.738e-2	0.995
	256×256	9.313e-6	2.003	2.752e-3	0.998	8.702e-3	0.998
	512×512	2.326e-6	2.001	1.377e-3	0.999	4.354e-3	0.999
Example 4.3(b)	16×16	2.643e-3	-	4.691e-2	-	1.483e-1	-
	32×32	6.501e-4	2.023	2.369e-2	0.986	7.491e-2	0.986
	64×64	1.613e-4	2.011	1.190e-2	0.994	3.762e-2	0.994
	128×128	4.043e-5	1.996	5.963e-3	0.996	1.886e-2	0.996
	256×256	1.009e-5	2.003	2.985e-3	0.998	9.440e-3	0.998
	512×512	2.524e-6	1.999	1.493e-3	0.999	4.723e-3	0.999
Example 4.3(c)	16×16	1.450e-3	-	2.631e-2	-	8.319e-2	-
	32×32	3.758e-4	1.948	1.351e-2	0.961	4.273e-2	0.961
	64×64	9.296e-5	2.015	6.836e-3	0.983	2.162e-2	0.983
	128×128	2.346e-5	1.986	3.440e-3	0.991	1.088e-2	0.991
	256×256	5.846e-6	2.005	1.725e-3	0.996	5.455e-3	0.996
	512×512	1.459e-6	2.002	8.634e-4	0.998	2.731e-3	0.998
Example 4.3(d)	16×16	2.062e-3	-	3.685e-2	-	1.165e-1	-
	32×32	5.102e-4	2.015	1.875e-2	0.974	5.930e-2	0.974
	64×64	1.292e-4	1.982	9.467e-3	0.986	2.994e-2	0.986
	128×128	3.217e-5	2.005	4.753e-3	0.994	1.503e-2	0.994
	256×256	8.070e-6	1.995	2.382e-3	0.997	7.533e-3	0.997
	512×512	2.015e-6	2.002	1.192e-3	0.998	3.771e-3	0.998
Example 4.3(e)	16×16	2.604e-3	-	3.096e-2	-	9.789e-2	-
	32×32	6.719e-4	1.954	1.584e-2	0.967	5.008e-2	0.967
	64×64	1.702e-4	1.981	8.003e-3	0.985	2.531e-2	0.985
	128×128	4.286e-5	1.990	4.022e-3	0.992	1.272e-2	0.992
	256×256	1.075e-5	1.995	2.017e-3	0.996	6.377e-3	0.996
	512×512	2.693e-6	1.997	1.010e-3	0.998	3.193e-3	0.998
Example 4.3(f)	16×16	2.372e-3	-	2.828e-2	-	8.944e-2	-
	32×32	6.131e-4	1.952	1.448e-2	0.966	4.578e-2	0.966
	64×64	1.559e-4	1.976	7.325e-3	0.983	2.316e-2	0.983
	128×128	3.923e-5	1.990	3.683e-3	0.992	1.165e-2	0.992
	256×256	9.847e-6	1.994	1.847e-3	0.996	5.840e-3	0.996
	512×512	2.466e-6	1.997	9.246e-4	0.998	2.924e-3	0.998

5 Conclusions

In this paper, we proposed an immersed finite element method for linear elasticity problems having displacement jump proportional to the normal stress across the interface. We used a uniform grid so that the interface is allowed to cut through the element. This scheme is convenient since no grid generation is necessary and it is easy to develop fast solver such as multigrid. Our scheme has fewer degrees of freedom than most of XFEM. Numerical results show optimal convergence orders in L^2, divergence norm and H^1-norm. Numerical experiments also show that our scheme does not lock, in other words,

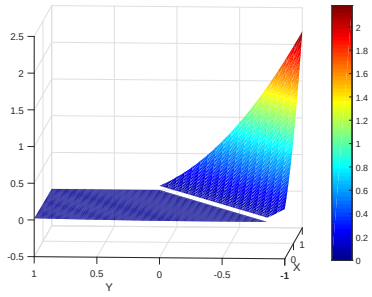

x-component of u for Example 4.3(a)

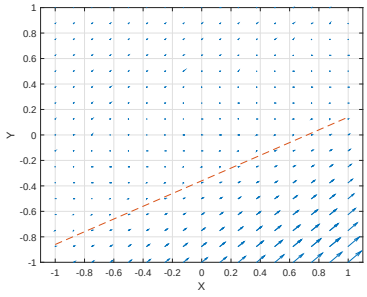

vector plot of u for Example 4.3(a)

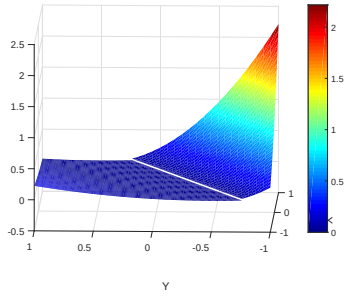

x-component of u for Example 4.3(b)

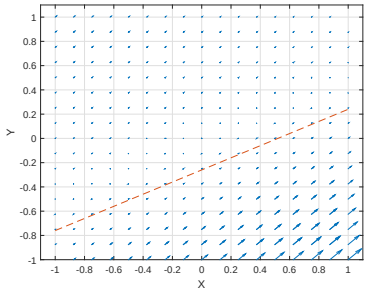

vector plot of u for Example 4.3(b)

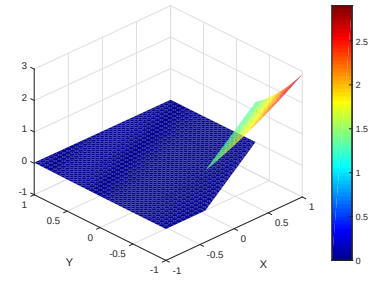

x-component of u for Example 4.3(c)

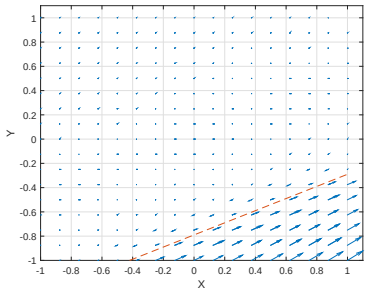

vector plot of u for Example 4.3(c)

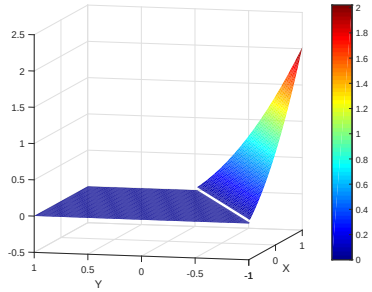

x-component of u for Example 4.3(d)

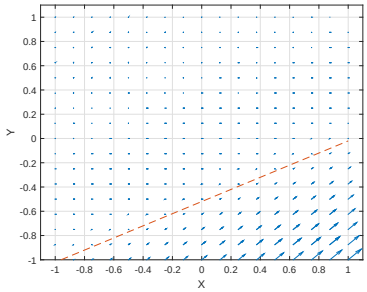

vector plot of u for Example 4.3(d)

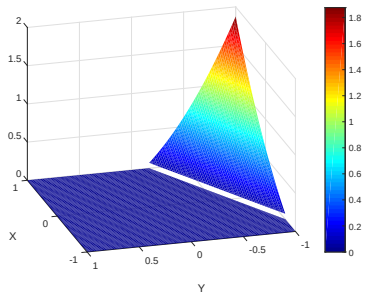

x-component of u for Example 4.3(e)

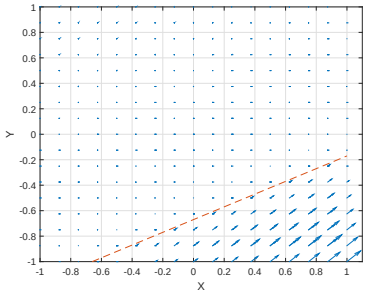

vector plot of u for Example 4.3(e)

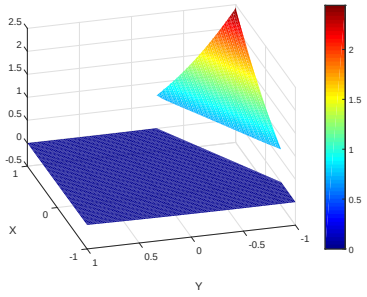

x-component of u for Example 4.3(f)

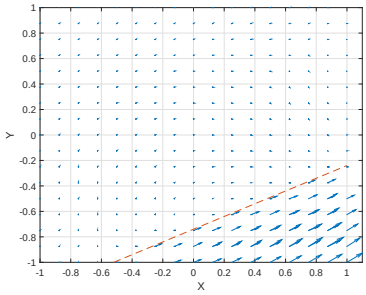

vector plot of u for Example 4.3(f)

Figure 5: Line interface, plots of u for Example 4.3.

the convergence rates of our method does not deteriorate even if the Poisson ratio approaches 1/2. For the future works, we will generalize it to 3-D problems, and consider other type of jump conditions such as crack propagation problems.

Acknowledgments

The authors are supported by grants from the National Research Foundatin of Korea (NRF, No. 2014R1A2A1A11053889).

References

[1] R. Becker, E. Burman and P. Hansbo, *A nitsche extended finite element method for incompressible elasticity with discontinuous modulus of elasticity*, Comput. Methods Appl. Mech. Eng., 198 (2009), pp. 3352–3360.

[2] T. Belytschko, N. Moës, S. Usui and C. Parimi, *Arbitrary discontinuities in finite elements*, Int. J. Numer. Methods Eng., 50 (2001), pp. 993–1013.

[3] S. C. Brenner and L.-Y. Sung, *Linear finite element methods for planar linear elasticity*, Math. Comput., 59 (1992), pp. 321–338.

[4] Y. Cao, Y. Chu, X. He and T. Lin, *An iterative immersed finite element method for an electric potential interface problem based on given surface electric quantity*, J. Comput. Phys., 281 (2015), pp. 82–95.
[5] K. S. Chang and D. Y. Kwak, *Discontinuous bubble scheme for elliptic problems with jumps in the solution*, Comput. Methods Appl. Mech. Eng., 200 (2011), pp. 494–508.
[6] S.-H. Chou, D. Y. Kwak and K. T. Wee, *Optimal convergence analysis of an immersed interface finite element method*, Adv. Comput. Math., 33 (2010), pp. 149–168.
[7] P. G. Ciarlet, Mathematical Elasticity, Vol. I, Volume 20 of Studies in Mathematics and Its Applications, 1988.
[8] J. Dolbow and T. Belytschko, *A finite element method for crack growth without remeshing*, Int. J. Numer. Meth. Eng., 46 (1999), pp. 131–150.
[9] R. S. Falk, *Nonconforming finite element methods for the equations of linear elasticity*, Math. Comput., 57 (1991), pp. 529–550.
[10] Y. Gong, B. Li and Z. Li, *Immersed-interface finite-element methods for elliptic interface problems with nonhomogeneous jump conditions*, SIAM J. Numer. Anal., 46 (2008), pp. 472–495.
[11] H. Groth, *Stress singularities and fracture at interface corners in bonded joints*, Int. J. Adhesion Adhesives, 8 (1988), pp. 107–113.
[12] J. Guedes and N. Kikuchi, *Preprocessing and postprocessing for materials based on the homogenization method with adaptive finite element methods*, Comput. Methods Appl. Mech. Eng., 83 (1990), pp. 143–198.
[13] A. Hansbo and P. Hansbo, *A finite element method for the simulation of strong and weak discontinuities in solid mechanics*, Comput. Methods Appl. Mech. Eng., 193 (2004), pp. 3523–3540.
[14] P. Hansbo, M. Larson and M. G. Larson, *A simple nonconforming bilinear element for the elasticity problem*, Trends in Computational Structural Mechanics, Citeseer, 2001.
[15] P. Hansbo and M. G. Larson, *Discontinuous galerkin and the crouzeix–raviart element: application to elasticity*, ESAIM: Math. Model. Numer. Anal., 37 (2003), pp. 63–72.
[16] X. He, T. Lin, Y. Lin and X. Zhang, *Immersed finite element methods for parabolic equations with moving interface*, Numer. Methods Partial Differential Equations, 29 (2013), pp. 619–646.
[17] S. Hou, Z. Li, L. Wang and W. Wang, *A numerical method for solving elasticity equations with interfaces*, Commun. Comput. Phys., 12 (2012), pp. 595–612.
[18] S. Hou, P. Song, L. Wang and H. Zhao, *A weak formulation for solving elliptic interface problems without body fitted grid*, J. Comput. Phys., 249 (2013), pp. 80–95.
[19] H. Jian, Y. Chu, H. Cao, Y. Cao, X. He and G. Xia, *Three-dimensional ife-pic numerical simulation of background pressure's effect on accelerator grid impingement current for ion optics*, Vacuum, 116 (2015), pp. 130–138.
[20] D. Y. Kwak, S. Jin, and D. Kyeong, *A stabilized p_1 immersed finite element method for the interface elasticity problems*, ESAIM: Math. Model. Numer. Anal., in press.
[21] D. Y. Kwak and J. Lee, *A modified p_1-immersed finite element method*, Int. J. Pure Appl. Math., 104 (2015), pp. 471–479.
[22] D. Y. Kwak, K. T. Wee and K. S. Chang, *An analysis of a broken p_1-nonconforming finite element method for interface problems*, SIAM J. Numer. Anal., 48 (2010), pp. 2117–2134.
[23] D. Leguillon and E. Sanchez-Palencia, Computation of Singular Solutions in Elliptic Problems and Elasticity, John Wiley & Sons, Inc., 1987.
[24] A. Lew, P. Neff, D. Sulsky and M. Ortiz, *Optimal bv estimates for a discontinuous galerkin method for linear elasticity*, Appl. Math. Research Express, 2004 (2004), pp. 73–106.
[25] Z. Li, T. Lin, Y. Lin and R. C. Rogers, *An immersed finite element space and its approximation*

capability, Numer. Methods Partial Differential Equations, 20 (2004), pp. 338–367.
[26] Z. Li, T. Lin and X. Wu, *New cartesian grid methods for interface problems using the finite element formulation*, Numerische Mathematik, 96 (2003), pp. 61–98.
[27] T. Lin, Y. Lin and X. Zhang, *Partially penalized immersed finite element methods for elliptic interface problems*, SIAM J. Numer. Anal., 53 (2015), pp. 1121–1144.
[28] T. Lin, D. Shen and X. Zhang, *A locking-free immersed finite element method for planar elasticity interface problems*, J. Comput. Phys., 247 (2013), pp. 228–247.
[29] T. Lin and X. Zhang, *Linear and bilinear immersed finite elements for planar elasticity interface problems*, J. Comput. Appl. Math., 236 (2012), pp. 4681–4699.
[30] W. Qiu and L. Demkowicz, *Mixed hp-finite element method for linear elasticity with weakly imposed symmetry*, Comput. Methods Appl. Mech. Eng., 198 (2009), pp. 3682–3701.
[31] B. Riviere, S. Shaw, M. F. Wheeler and J. R. Whiteman, *Discontinuous galerkin finite element methods for linear elasticity and quasistatic linear viscoelasticity*, Numerische Mathematik, 95 (2003), pp. 347–376.
[32] E. Samaniego and T. Belytschko, *Continuum-discontinuum modelling of shear bands*, Int. J. Numer. Methods Eng., 62 (2005), pp. 1857–1872.
[33] N. Sukumar, D. L. Chopp, N. Moës and T. Belytschko, *Modeling holes and inclusions by level sets in the extended finite-element method*, Comput. Methods Appl. Mech. Eng., 190 (2001), pp. 6183–6200.
[34] L. Wang, S. Hou and L. Shi, *A numerical method for solving 3d elasticity equations with sharp-edged interfaces*, Int. J. Partial Differential Equations, 2013 (2013).
[35] Z. Zhong and S. A. Meguid, *On the imperfectly bonded spherical inclusion problem*, J. Appl. Mech., 66 (1999), pp. 839–846.
[36] O. C. Zienkiewicz and R. L. Taylor, The Finite Element Method: Solid Mechanics, Vol. 2, Butterworth-Heinemann, 2000.